

Liquids with High Compressibility

Beibei Lai, Siyuan Liu, John Cahir, Yueting Sun, Haixia Yin, Tristan Youngs, Jin-Chong Tan, Sergio F. Fonrouge, Mario G. Del Pópolo, José L. Borioni, Deborah E. Crawford, Francesca M. Alexander, Chunchun Li, Steven E. J. Bell, Barry Murrer, and Stuart L. James*

Compressibility is a fundamental property of all materials. For fluids, that is, gases and liquids, compressibility forms the basis of technologies such as pneumatics and hydraulics and determines basic phenomena such as the propagation of sound and shock waves. In contrast to gases, liquids are almost incompressible. If the compressibility of liquids could be increased and controlled, new applications in hydraulics and shock absorption could result. Here, it is shown that dispersing hydrophobic porous particles into water gives aqueous suspensions with much greater compressibilities than any normal liquids such as water (specifically, up to 20 times greater over certain pressure ranges). The increased compressibility results from water molecules being forced into the hydrophobic pores of the particles under applied pressure. The degree of compression can be controlled by varying the amount of porous particles added. Also, the pressure range of compression can be reduced by adding methanol or increased by adding salt. In all cases, the liquids expand back to their original volume when the applied pressure is released. The approach shown here is simple and economical and could potentially be scaled up to give large amounts of highly compressible liquids.

become occupied by molecules of the liquid.^[3] Either process would result in a decrease in the overall volume of the liquid. Such processes could potentially be reversible or irreversible depending on the nature of the chemistry involved. Although liquids that contain empty spaces may seem counterintuitive, recently such liquids, termed “porous liquids” (PLs), have begun to emerge as a new class of fluid materials.^[4,5] They have been noted for their ability to absorb large amounts of gases into their empty pores, but their compressibility has not yet been explored.

A promising class of PLs with regard to compressibility studies are Type-III PLs, which are formed by dispersing small particles of solid porous materials into a carrier liquid whose molecules are size-excluded from the pores of the particles.^[4] Type-III PLs are promising for achieving compressibility because the total void volume can be relatively high (e.g., up to around 20%), and because

their design can benefit from existing physical knowledge of their porous solid components. For example, some porous solids are known to be compressible, that is, they collapse into denser forms under applied pressure.^[6] Therefore, Type-III PLs that consist of dispersions of particles of such solids in carrier liquids could also

1. Introduction

Strategies to create a liquid with high compressibility can be based on engineering empty spaces in the liquid.^[1,2] When pressure is applied, these empty spaces could: i) collapse, or ii)

B. Lai, S. Liu, J. Cahir, D. E. Crawford, F. M. Alexander, C. Li, S. E. J. Bell, B. Murrer, S. L. James
School of Chemistry and Chemical Engineering
Queen's University Belfast
Belfast, Northern Ireland BT9 5AG, UK
E-mail: s.james@qub.ac.uk


Y. Sun, H. Yin
School of Engineering
University of Birmingham
Birmingham B15 2TT, UK

T. Youngs
ISIS Pulsed Neutron and Muon Source
STFC Rutherford Appleton Laboratory
Didcot OX11 0QX, UK

J.-C. Tan
Department of Engineering Science
University of Oxford
Oxford OX1 3PJ, UK

S. F. Fonrouge, M. G. D. Pópolo
ICB-CONICET & Facultad de Ciencias Exactas y Naturales
Universidad Nacional de Cuyo
Mendoza CP5500, Argentina

J. L. Borioni
Departamento de Química Orgánica
Facultad de Ciencias Químicas
Universidad Nacional de Córdoba
Córdoba X5000HUA, Argentina

 The ORCID identification number(s) for the author(s) of this article can be found under <https://doi.org/10.1002/adma.202306521>

© 2023 The Authors. Advanced Materials published by Wiley-VCH GmbH. This is an open access article under the terms of the Creative Commons Attribution License, which permits use, distribution and reproduction in any medium, provided the original work is properly cited.

DOI: 10.1002/adma.202306521

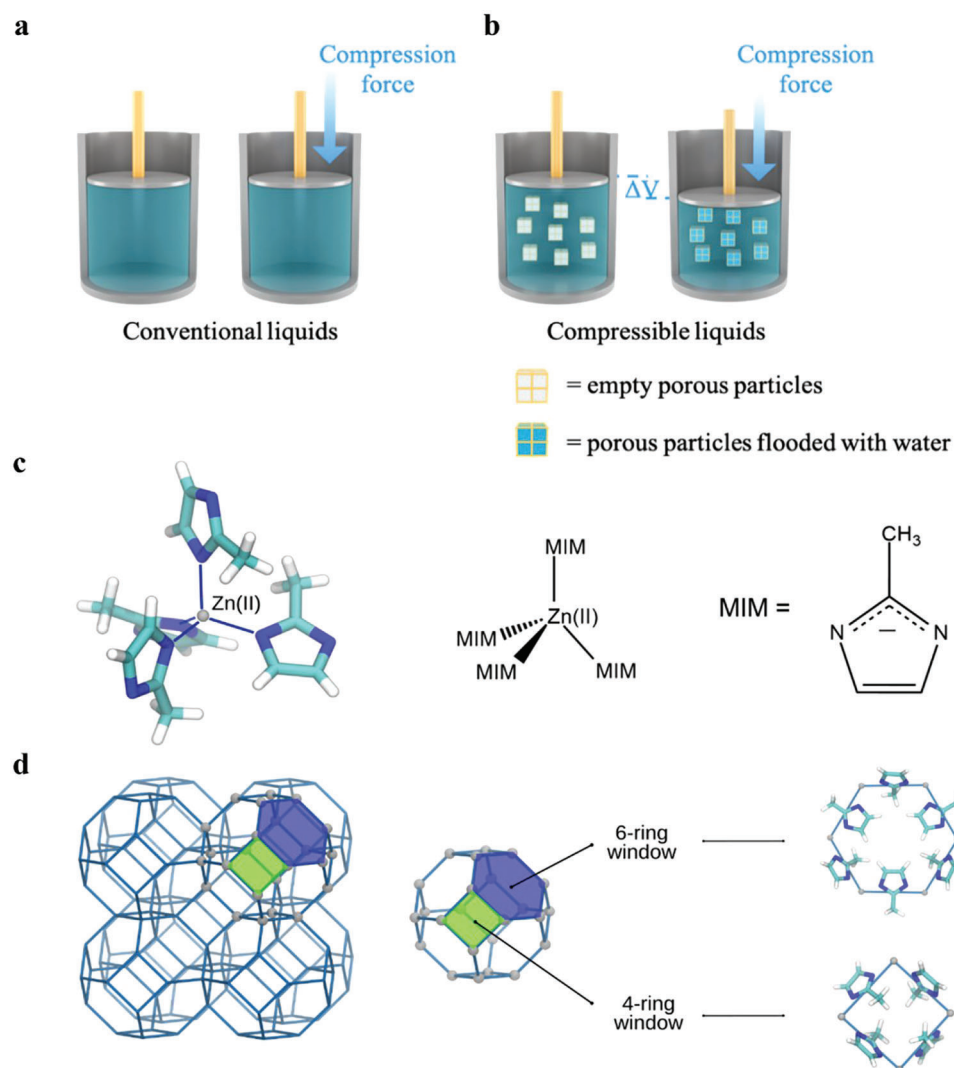


Figure 1. The principle demonstrated here to achieve high compressibility in a liquid. a) Conventional liquids are almost incompressible, this is because there is very little space between the molecules of the liquid. b) To create a compressible liquid, porous particles (yellow) are dispersed into a liquid phase. The molecules of the liquid do not enter the porous particles at low pressures and so the particles remain empty, that is, the liquid phase is porous and a substantial proportion of it is empty space (white). However, when pressure is applied the liquid is forced into the pores of the dispersed particles causing a decrease in the total volume, that is, resulting in high compressibility. c) The molecular structure of ZIF-8, a material with hydrophobic pores used as the porous particles in this work. d) Representation of the empty pores of ZIF-8 which can potentially be accessed by molecules through the open windows.

be expected to be compressible. Alternatively, as demonstrated here, compressible liquids could be based on Type-III PLs in which the application of pressure forces molecules of the liquid into the dispersed porous particles (Figure 1a,b). However, realizing such behavior will require a very fine control over the size-exclusion of the liquid molecules, which may be challenging to achieve. A more tractable variation on this approach is to use Type-III PLs in which the exclusion of the liquid phase from the pores is not based on size-exclusion but on solvophobicity. In particular, using pressure to force water into the pores of a range of hydrophobic porous solids has been studied in the literature, including modifying the pressure range of intrusion by adding alcohol or salts.^[7–18] This provides a basis for forming compress-

ible liquids by dispersing particles of hydrophobic porous solids in aqueous phases.

2. Results and Discussion

2.1. Design and Synthesis

ZIF-8 is a solid, crystalline metal–organic framework material which is highly porous ($\approx 60\%$ of its total volume is empty space, Figure 1c,d).^[19] It is a highly hydrophobic material. In particular, its internal pores have very low water affinity,^[20] and it exhibits a high water-contact angle^[21] (142°) on its external surface. Consequently, water does not enter its pores at ambient

pressure. However, water can be forced in at pressures of ≈ 200 – 300 bar.^[7–17] We therefore sought to disperse particles of ZIF-8 into water to form a homogeneous dispersion, in the expectation that such a dispersion should exhibit unusually high compressibility, according to our strategy outlined above (Figure 1). However, to obtain a stable, homogeneous dispersion of a solid in a liquid, the solid particles should normally be as small as possible to exhibit a high external surface area (per unit volume) and thereby maximize interactions between the particles and the liquid phase in which they are dispersed. Also, the external surface of the particles should ideally exhibit attractive interactions with the liquid. Indeed, stable dispersions of the hydrophobic porous solid silicalite-1 have recently been reported based on these two considerations.^[22] Further, stability can be increased by matching the densities of the liquid phase and the dispersed particles. ZIF-8, as prepared by standard methods (crystallization from solution), here designated ZIF-8S, normally consists of relatively large particles (several hundred nm), has hydrophobic external surfaces as noted above and low density (crystallographic density 0.95 g cm^{-3}).^[19] Correspondingly, we found that ZIF-8S did not form stable dispersions in water. Specifically, after vigorous stirring for several hours to disperse the solid, the solid particles floated to the top of the water (creamed) within 2 days. Scanning electron microscopy (SEM) of the solid ZIF-8S showed polyhedral particles of ≈ 400 nm (Figure S1, Supporting Information). Dynamic light scattering (DLS) of the aqueous dispersion before creaming occurred showed particles principally of ≈ 1000 nm suggesting there is aggregation of the particles in water. Consistent with the low stability of this dispersion, and in agreement with literature,^[20] the external surface of the ZIF-8S material was confirmed to be strongly hydrophobic as indicated by a high water-contact angle of $139.45 \pm 2.54^\circ$ (Figure S11b, Supporting Information). The stability of these dispersions was deemed insufficient for performing compression studies.

To improve the dispersion stability, we sought an alternative form of ZIF-8. It has been previously noted that mechanochemical, solvent-free synthesis of related porous materials can give rise to smaller particles than standard solution-based methods.^[23] We therefore investigated ZIF-8 made by this less conventional method (specifically by using solvent-free twin screw extrusion, as reported previously).^[24] We further noted that if the reaction conditions were selected such that incomplete conversion of the reactants to ZIF-8 occurred,^[25] then the product, here termed ZIF-8E, was found to contain ≈ 15 wt% of the basic zinc carbonate reactant, $[\text{ZnCO}_3]_2[\text{Zn}(\text{OH})_2]_3$, as shown by TGA and solid state ^{13}C NMR spectroscopy. Being more dense (crystallographic density = 3.5 g cm^{-3}) than ZIF-8,^[26] the presence of $[\text{ZnCO}_3]_2[\text{Zn}(\text{OH})_2]_3$ should prevent the creaming of the particles and so improve the stability of aqueous dispersions. ZIF-8E was found to consist of relatively small particles (30–200 nm) as revealed by SEM, transmission electron microscopy, and DLS (Figures S2 and S14, Supporting Information). Analysis of particle size distribution by DLS coupled with visual nanoparticle tracking for aqueous dispersions gave qualitatively similar differences in particle size distribution between ZIF-8S and ZIF-8E (Figure S13, Supporting Information). Analysis by confocal Raman spectroscopy did not detect any $[\text{ZnCO}_3]_2[\text{Zn}(\text{OH})_2]_3$ on the surfaces of the particles of ZIF-8E, suggesting that it is contained

within the particles. This is consistent with the mechanochemical method of synthesis in which particles react initially on their surfaces, and remaining unreacted material is expected to be buried within the particles.^[27] Correspondingly, the presence of $[\text{ZnCO}_3]_2[\text{Zn}(\text{OH})_2]_3$ in ZIF-8E made little or no difference to the water-contact angle ($121.54 \pm 6.65^\circ$, Figure S11c, Supporting Information) or the zeta potential of ZIF-8E compared to those of ZIF-8S. However, as hoped, ZIF-8E was easily dispersed into water at 12.5 wt% by vigorous magnetic stirring for 2–4 h to form a milk-like dispersion, hereafter designated as “Compressible Liquid 1” (CL1). The physical stability of the dispersion was quantified through space- and time-resolved extinction profiles generated using 870 nm light (Figure S15, Supporting Information). The derived instability index for the aqueous ZIF-8S dispersion was 0.55 whereas for CL1 it was 0.21 (Figure S17, Supporting Information) confirming the greater stability of the latter. ZIF-8E could be recovered from CL1 by filtration, and powder X-ray diffraction analysis showed that it retained its crystal structure even after CL1 had aged for 1 week in air. CL1 was stable to sedimentation for at least 11 days and therefore amenable to study by compression experiments. Also, despite the presence of $[\text{ZnCO}_3]_2[\text{Zn}(\text{OH})_2]_3$, ZIF-8E exhibits at least 85% of the pore volume of ZIF-8S, so that the degree of compression of CL1 should still be far higher than that of conventional liquids. Overall, the increased physical stability of aqueous dispersions of ZIF-8E compared to those of ZIF-8S can be attributed to the increase in particle density and reduced particle size.

2.2. Compression Experiments

The volume change of CL1 was measured using an Instron testing machine with a stainless-steel chamber to apply hydrostatic pressure to the sample inside (Figure 2 and Figure S21, Supporting Information). Pressure was increased from 1 bar to 500 bar at a constant rate of 0.5 mm min^{-1} and then decreased to 1 bar at the same rate. Figure 2a shows that the volume of CL1 had reduced by $\approx 7\%$ at 500 bar, with most of this compression ($\approx 4\%$) occurring above 220 bar, the pressure at which water starts to be forced into ZIF-8. In contrast, under the same conditions, pure water only gave a compression of 2.3% at 500 bar, approximately one-third that of CL1. Note that for compressible liquids, the amount of compression is governed by the total pore volume available and it therefore can be adjusted by changing the amount of ZIF-8E dispersed in CL1. Correspondingly, doubling the amount of ZIF-8E in CL1 to give a 25 wt% dispersion was found to result in a compression of $\approx 11\%$ at 500 bar, and simultaneously gave a wider range of working pressure (Figure S25, Supporting Information). Also notable is that the presence of $[\text{ZnCO}_3]_2[\text{Zn}(\text{OH})_2]_3$ in CL1 does not dramatically affect the ease with which water molecules can enter the ZIF-8E pores, since the observed intrusion pressure for CL1 is very similar to that of pure ZIF-8.^[7,9]

The compressibility (β), defined as the relative volume change in response to the change in pressure, of CL1 is plotted in Figure 2a, bottom. CL1 has a similar compressibility to pure water at pressures above or below the intrusion process, but deviates greatly from that of water and gains its highest compressibility during the intrusion process (Figure 2a). Specifically, the compressibility of CL1 peaks at a value of around 10 GPa^{-1} , twenty

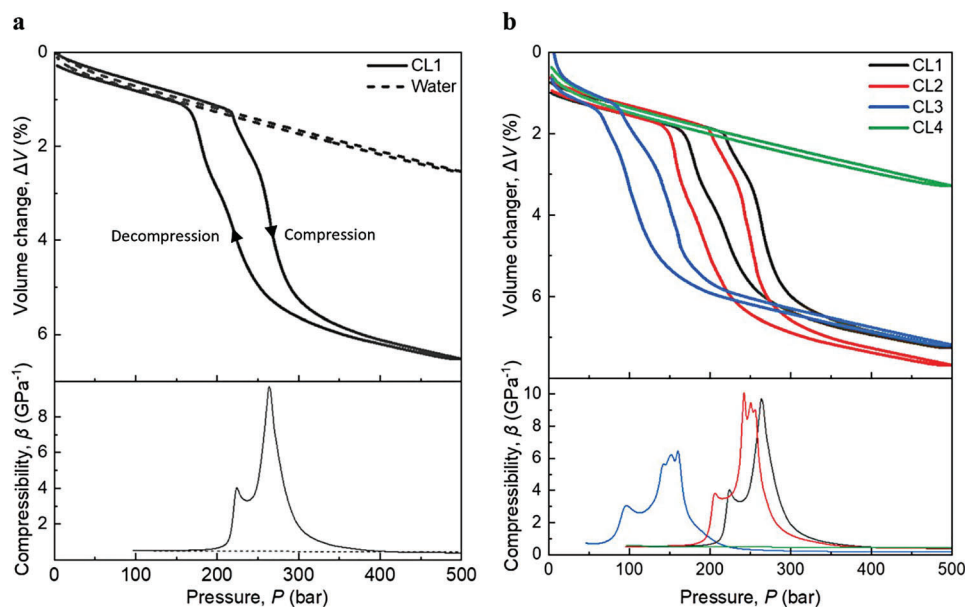


Figure 2. Compression tests on various compressible liquids, including the volume changes during compression–decompression cycles, and compressibility at different pressures. a) Comparison between CL1 (ZIF-8 dispersed in H₂O) and pure water, b) Comparison between different compressible liquids (CL1 to CL4) containing different concentrations of methanol (0, 1, 5, or 10 wt%). Replacing part of the water with methanol makes intrusion of the liquid into the porous particles easier and thus the compression occurs at lower pressures. Over certain pressure ranges, the compressibility of CLs is more than an order of magnitude greater than that of pure water or methanol solutions.

times that of pure water (0.5 GPa⁻¹). The compressibility of a material at a given pressure is often reported as its reciprocal quantity, the bulk modulus, which is plotted in Figure S22, Supporting Information. As expected, the increase in compressibility corresponds to a remarkably large (20-fold) reduction of bulk modulus, from above 2 GPa for pure water to ≈0.1 GPa for CL1. At pressures above and below the intrusion process, the bulk moduli of CL1 and water are similar, showing that the compression occurring in these regions is that of the interstitial water in CL1. The double maxima in the compressibility data show clearly that the compression occurs in two steps. This can be related to a structural change in the ZIF-8 which occurs during the filling process as discussed further below.

The compression of CL1 was rapidly reversed when the pressure was reduced back to 1 bar, with good reproducibility being observed over multiple cycles (Figure S26, Supporting Information), although in some cases a period of relaxation was required for full recovery.^[8] Hysteresis was observed in the pressure–volume change relationship (Figure 2a), (consistent with previous studies of water intrusion into ZIF-8)^[8,11] indicating that shock absorption might be a potential application of compressible liquids. During the decompression process, the compressibility and bulk modulus exhibit similar trends to those in compression, except that the highest compressibility is gained at a relatively lower pressure due to the hysteresis (Figure S22, Supporting Information).

To examine how the pressure that offers the high compressibility could be varied, experiments were conducted with a small amount of water replaced by methanol, specifically 1, 5, or 10 wt%, to give CL2, CL3, and CL4, respectively. In each case, homogeneous 12.5 wt% dispersions of ZIF-8E formed readily with only ≈10 min stirring. Their compressibilities were all simi-

lar to each other in terms of peak values and the width of the pressure window that offers high compressibility (Figure S27, Supporting Information). However, as hoped, the presence of methanol lowered the intrusion pressure substantially to around 205 bar (CL2) and 90 bar (CL3), confirming that the high compressibility can be gained at substantially lower pressure through this strategy (Figure 2b).^[9] For greater methanol content such as 10 wt% the compression was linear over the full pressure range, and CL4 actually behaves similarly to the pure water–methanol solvent (i.e., not containing ZIF-8E, Figure S27, Supporting Information). This suggests that ZIF-8E already absorbed the solvent under ambient conditions before the compression began. Therefore, a low methanol concentration is required to make effective compressible liquids. The high compressibility can also be gained at an increased pressure by dissolving salt in the liquid, for example, CL5, made from 12.5 wt% ZIF-8E dispersed in 2 M NaCl solution (Figure S28, Supporting Information), consistent with previous findings on the osmotic effect regarding electrolyte intrusions of ZIF-8.^[18] Therefore, this generic type of compressible liquid is versatile and can be designed to exhibit high compressibility at a predefined pressure.^[9,10,28] It is notable that the compressibilities of CL1–4 of up to 10 GPa⁻¹ are all far greater than those of any conventional liquids, or mixtures thereof, which are usually less than 1 GPa⁻¹ (Figure S29, Supporting Information).

2.3. Neutron Scattering Experiments

To explore any potential structural changes in the liquid during compression, CL1 and CL3 were analyzed by neutron scattering during the compression process. This was of particular interest because ZIF-8 has previously been reported to change structure

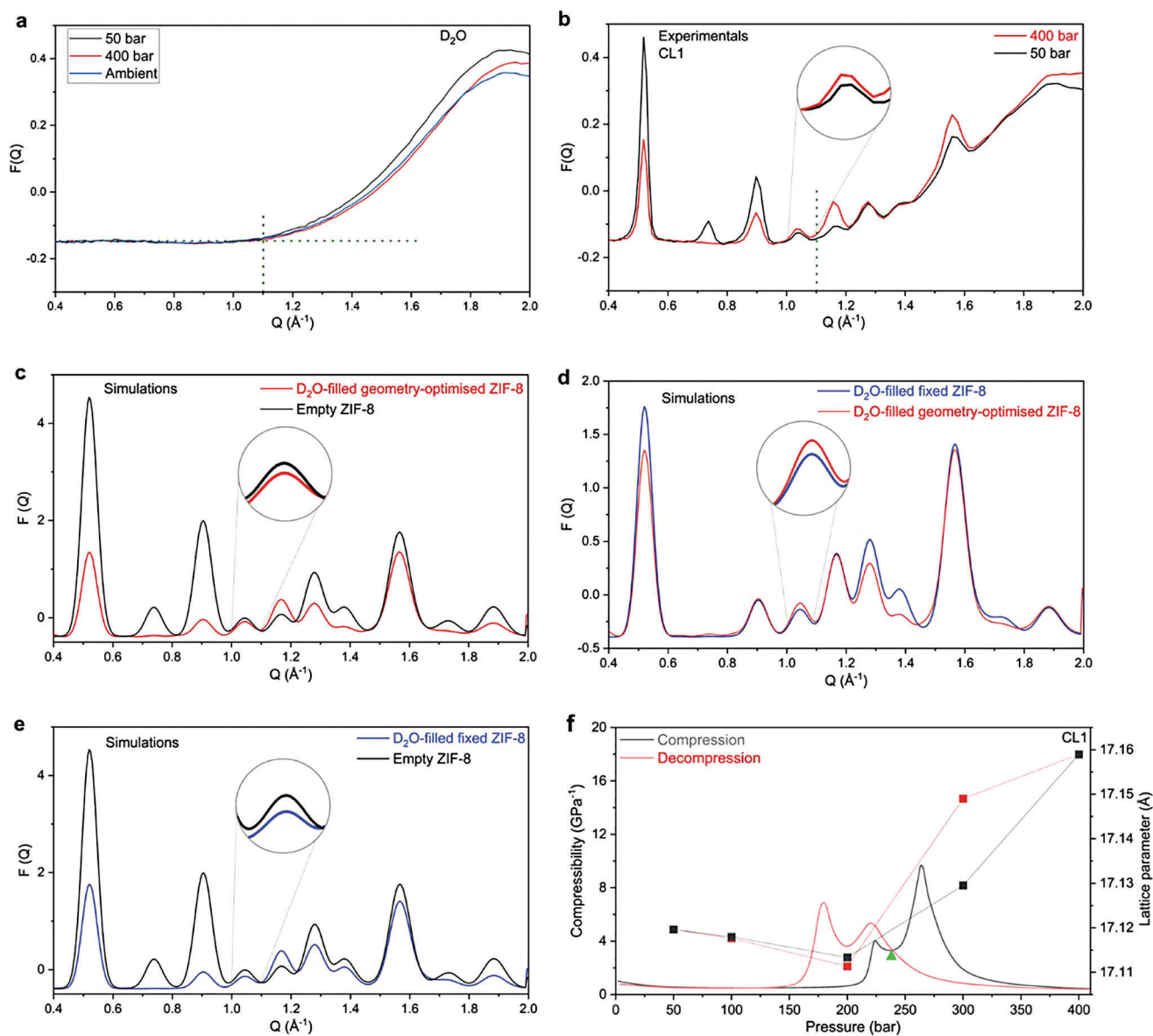


Figure 3. Experimental small-angle neutron scattering patterns for D_2O , CL1, and simulated neutron scattering patterns of the empty ZIF-8 and D_2O -filled ZIF-8 structures. a) Experimental neutron scattering patterns at 50 and 400 bar for D_2O ; b) the experimental neutron scattering patterns at 50 and 400 bar for CL1; c) simulated data for the empty ZIF-8 and D_2O -filled geometry-optimized ZIF-8 structure; d) simulated data for the D_2O -filled fixed ZIF-8 and D_2O -filled geometry-optimized ZIF-8; and e) simulated data for the D_2O -filled fixed ZIF-8 and empty ZIF-8. Q (\AA^{-1}) indicates the scattering vector. f) Overlay of the variation with pressure of the lattice parameter and compressibility with pressure of CL1 during compression (black) and decompression (red). The turning point between the decrease and increase in lattice parameter is consistent with the local minimum (green \blacktriangle) in compressibility, indicating that the two-step filling process can be related to structural change in the ZIF-8 particles.

under pressure under some conditions, a process referred to as a gate opening/closing mechanism.^[29] It can be noted that although a structural change such as this can contribute to hysteresis, hysteresis has also been observed during water intrusion into structurally rigid hydrophobic porous materials.^[30] Data (from $Q = 0.02\text{--}50 \text{ \AA}^{-1}$, where Q is the scattering vector) were collected on the near intermediate range order diffractometer (ISIS Neutron and Muon Source). The experimental set-up is described in Figure S30, Supporting Information. Deuterated water (D_2O) and deuterated methanol (CD_3OD) were used as the liquid com-

ponents to avoid high background scattering from H atoms. As the pressure was increased, data were collected at 50, 100, 200, 300, and 400 bar and again at the same points while the pressure was subsequently decreased. Each pressure point was maintained for 3 h to allow for data collection, giving a total experiment run time of 27 h.

Small-angle neutron scattering diffraction patterns for CL1 are shown in Figure 3b. The expected Bragg peaks corresponding to ZIF-8 are observed from $Q = 0.5\text{--}1.7 \text{ \AA}^{-1}$,^[31] superimposed on a broad hump from $Q = 1.2\text{--}2.0 \text{ \AA}^{-1}$ which is due to the

bulk D₂O liquid phase (Figure 3a, black). As the pressure was increased from 50 to 400 bar, the intensities of the individual peaks due to ZIF-8 systematically increased, systematically decreased or remained unchanged (Figure 3b, red). Changes in peak intensity can in general be related to structural changes in the ZIF-8 framework and/or to changes in scattering contrast due to the pore-filling by D₂O. Most notable for the following discussion are peaks at $Q = 0.52, 0.74, \text{ and } 0.91 \text{ \AA}^{-1}$, which all decreased in intensity, and the peak at 1.04 \AA^{-1} which increased in intensity, as discussed below. When the pressure was decreased from 400 to 100 bar, the intensities of all peaks returned to their original values, showing that the structure returns to its original state. The pressure range over which the changes in peak intensity occurred corresponded closely to the process of water intrusion as determined from the compression experiments described above. Similar overall behavior was observed for CL3 (Figure 2b), except that the changes in peak intensity occurred at lower pressure, again consistent with the compression press experiments described above (Figure S27, Supporting Information).

2.4. Neutron Scattering Simulation and Interpretation

In order to understand the reason for the experimentally-observed changes in peak intensities we generated computational structural models and thereby simulated the neutron scattering patterns of empty ZIF-8 and D₂O-filled ZIF-8, while either fixing the ZIF-8 framework or allowing its geometry to equilibrate after the pore filling process. The initial ZIF-8 atomic coordinates used were based on a unit cell previously determined from X-ray diffraction data^[32] and equilibration was done using an infinite periodic repeating $2 \times 2 \times 2$ supercell. A combination of canonical Monte Carlo (MC) and molecular dynamics (MD) methods was used to allow the structure to optimize and neutron scattering data were simulated using Dissolve (1.0.0) software^[33] (see Figure S58, Supporting Information, for details). 640 water molecules were loaded in the cavities of the supercell to simulate the filled structure, a value calculated from the degree of compression observed experimentally.

First, the combined effects of framework structural equilibration and D₂O-filling were examined. Specifically, a comparison was made between the predicted neutron scattering patterns for the crystallographically-determined ZIF-8 structure in its empty state (Figure 3c, black trace) with the pattern for the modeled structure after it had been filled with D₂O, and after the geometries of both the framework and the contained water molecules had been allowed to equilibrate (Figure 3c, red trace). The structural flexibility of the ZIF-8 framework is known to arise from rotation of the methylimidazole groups, and is conventionally parameterized by the angle θ between the planes defined by the four Zn ions^[34] that define a four-membered pore opening. During the modeling of the filling and associated structural equilibration process, the average θ value reduced from 61.0° (Figure S57, Supporting Information) to 55.9° (Figure S68, Supporting Information). It should be noted that the simulation method used here does not encompass the bulk D₂O outside the ZIF-8 nor therefore the broad hump which this generates in the neutron scattering data. Since this hump affects the ZIF-8 peak intensities at high Q , and because it has been found experimentally to

vary with applied pressure,^[35] we confine our discussion here to the four peaks with $Q < 1.1 \text{ \AA}^{-1}$. For the first three peaks ($Q = 0.52, 0.74, \text{ and } 0.91 \text{ \AA}^{-1}$) there is good qualitative agreement with the experimental data, in that all peaks reduce in intensity (the 0.74 \AA^{-1} peak vanishes altogether). Interestingly, whereas the peak at 1.04 \AA^{-1} increased in intensity during the experimental filling process, in contrast, the simulation predicts that it too should decrease. To gain further insight into the reason for this discrepancy, we conducted simulations that would distinguish between the effects of a scattering contrast change due to the pores filling with D₂O, and the effects of equilibration in the ZIF-8 framework structure itself. Specifically, by comparing the simulated neutron scattering data for empty, fixed ZIF-8 with that for D₂O-filled fixed ZIF-8, the effect of pore filling alone can be seen (Figure 3e). The filling effect is predicted to decrease the intensities of all peaks below 1.1 \AA^{-1} , and therefore this phenomenon does not account for the experimentally-observed increase in the 1.04 \AA^{-1} peak. Further, by comparing the simulated data for the D₂O-filled fixed ZIF-8 structure ($\theta = 61.0^\circ$) with that of the D₂O-filled equilibrated ZIF-8 structure ($\theta = 55.9^\circ$) the effect of the framework structural change alone can be seen (Figure 3d). This reveals that the decrease in θ causes the intensity of the peak at 1.04 \AA^{-1} to increase (see also Figure S70 and Table S20, Supporting Information). This suggests that the experimentally-observed increase in intensity at 1.04 \AA^{-1} is due to a framework structural change, specifically a decrease in the angle θ . It can be noted that the 1.04 \AA^{-1} peak is unique amongst peaks with $Q < 1.1 \text{ \AA}^{-1}$ in that pore-filling and decrease in θ have mutually opposite effects on its intensity. Therefore, it is particularly diagnostic in distinguishing between the effects of these two aspects on the experimental neutron scattering data. Overall, while we note the limitations of this simulation procedure (specifically, the effects of background bulk D₂O, pressure, and potential organization of D₂O molecules in the pores are not accounted for) the results point to a change in structure (reduction of θ) occurring during the filling process. This is in agreement with predictions made previously with regard to the effects of water-filling in ZIF-8, although the specific underlying mechanism of how water molecules initiate this structural change remains to be elucidated.^[8] As discussed below, this structural change has some bearing on the observation of hysteresis.

As mentioned above, each of the compression and decompression processes occurs in two distinct steps as shown in the compressibility data (Figure 3f). The neutron scattering analysis reveals that this behavior can be related to the structural change which occurs in the ZIF-8 framework. In particular, analysis of the lattice parameter (i.e., the edge length of the cubic unit cell), as derived from variation in the position of the peak at $\approx Q = 0.52 \text{ \AA}^{-1}$, shows that during the intrusion, there is initially a slight decrease in the lattice parameter (between 50 and 200 bar) followed by a larger increase (above 200 bar). Similar behavior has been seen during intrusion of water into bulk ZIF-8 material.^[11] Within the precision of these measurements (i.e., measurements were only made at 50, 100, 200, 300, and 400 bar), the position of the turning point in the size of the lattice parameter is consistent with the local minimum observed in the compressibility data at ≈ 235 bar. Therefore, we suggest that the two-step intrusion relates to structural change in ZIF-8 during the process. We note that the change in structure occurs, within the precision of

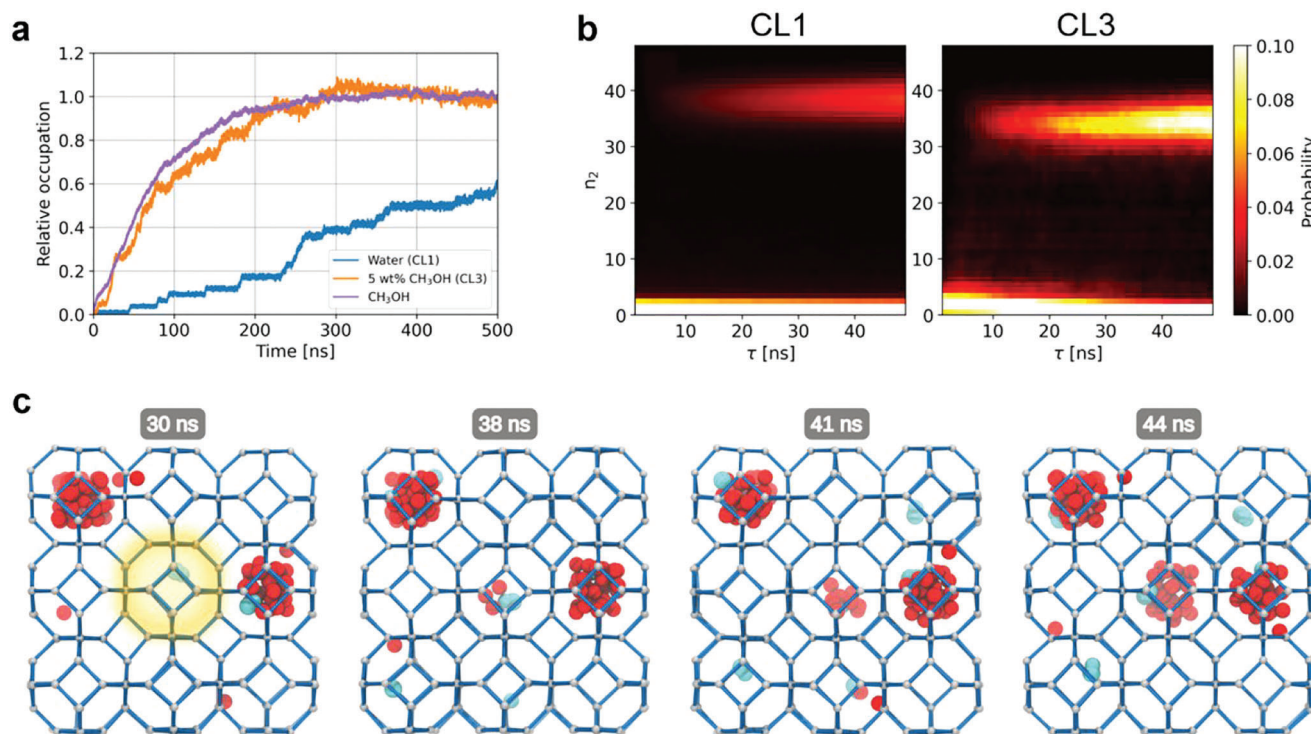


Figure 4. a) Evolution of fractional saturation per cavity (instantaneous number of molecules divided by the average number of molecules at saturation) of a ZIF-8 nanoparticle as solvent molecules intrude during compression simulations at 300 K and 800 bar. The stepwise intrusion of water in CL1 contrasts with the smoother and faster intrusion in the case of CL3. A simulation of the nanoparticle in pure methanol is included as a reference. b) Probability that a ZIF-8 cavity containing a single water (left) or methanol (right) molecule will have n_2 molecules after time τ . These probabilities were computed from compression simulations of the nanoparticle in neat water (CL1, left) and a 5 wt% methanol mixture (CL3, right). c) Simulation snapshots of a nucleation event where a single methanol molecule in the central cavity (yellow spot) precedes the formation of a subcritical cluster and the subsequent saturation of the cavity. A video and snapshots of other nucleation events induced by methanol are available in Figure S55, Supporting Information.

these experiments, between the two steps of the intrusion process, which might explain the origin of the two steps. However, we also note the previous work^[16] that has shown that the water intrusion pressure into ZIF-8 can vary with particle size, with smaller particles (e.g., 90 nm) absorbing at lower pressures than larger ones (e.g., 130 nm). Since ZIF-8E consists of a range of particle sizes (30–200 nm), this could also be the origin of the double-peak. Indeed related experiments in the literature with ZIF-8 did not show a double peak.^[11] It can be noted that similar two-step behavior is observed during decompression of CL1 (Figure 3f) and for compression and decompression of CL3 (Figure S35, Supporting Information).

2.5. Molecular Modeling

To gain molecular-level insight into the intrusion process, including how methanol lowers the intrusion pressure, atomistic Molecular Dynamics simulations were conducted for the instantaneous compression of a system consisting of a ZIF-8 nanoparticle suspended in water, methanol, or mixtures thereof, at 300 K and 1, 500, 800, or 1000 bar (for more details see Figures S50 and S51, and Table S19, Supporting Information). This nanoparticle had the shape of a cube of edge length 51 Å, corresponding to 3 unit cells (i.e., a $3 \times 3 \times 3$ supercell matrix), with

any surface-dangling vacant Zn coordination sites capped with 2-methylimidazolate ligands, and containing a total of 35 well-defined pores (Figure S50, Supporting Information).

Where the liquid phase was pure water (CL1) intrusion into the empty pores occurred in a stepwise manner, characterized by sudden bursts of water molecules entering from either the bulk water or from adjoining pores that had reached full occupation (Figure 4a). In contrast, the system that contained 5 wt% methanol (CL3) was found to fill the pores more quickly and more smoothly (Figure 4a). These trends continued for systems with greater proportions of methanol (e.g., pure methanol, Figure 4a and CL4, Figure S52, Supporting Information), with an intrusion rate comparable to that of neat methanol. Also notable for CL3 was that the methanol/water ratio in the pores was found to be greater than that in the bulk solution during both the initial and final stages of the intrusion process (Figure S52, Supporting Information), in spite of the much slower diffusion rate of confined methanol compared to that of water (Figures S46 and S47, Supporting Information). This partition of the methanol and water is consistent with the hydrophobic nature of ZIF-8 pores.

Analysis of the intrusion process involving CL3 suggests that empty cavities fill rapidly once a single methanol molecule enters them (Figure 4b,c and Figure S55, Supporting Information). This tendency was quantified by calculating the conditional probability that a cavity reaches occupation by n_2 molecules

after some time τ , given an initial occupation by n_1 water and/or methanol molecules. Figure 4b shows that cavities in CL3 were more likely to fill within 50 ns when n_1 corresponded to one methanol molecule, than for CL1 (where n_1 corresponds to one water molecule). Moreover, methanol enhanced the formation of small solvent clusters at short τ . These observations point to methanol molecules acting as nucleation seeds that facilitate the filling of the particle cavities, which in turn lowers the intrusion pressure.

It can be noted that the trends in variation of the angle θ within the ZIF-8 framework that were observed in the neutron scattering simulation studies described above (based on an infinite periodic ZIF-8 lattice), were also observed in these molecular dynamics studies (which are based on small suspended ZIF-8 particles), showing good agreement between these two modeling approaches.

3. Conclusion

While liquids have traditionally been regarded as poorly compressible, we show that the recent advent of porous liquids^[4,36] opens up strategies for making liquids with high compressibility. In this proof-of-principle work, and based on existing knowledge of water intrusion into hydrophobic porous solids, we have exemplified a group of compressible liquids based on ZIF-8E dispersed in various aqueous phases, in which the degree of compression is much greater than for any existing liquids. Also, using this strategy, the pressure range and degree of compression are shown to be tunable. In situ neutron scattering and molecular dynamics modeling have given insights into the structural changes and molecular-scale processes occurring during compression. Compressible liquids may potentially be formulated through a number of general strategies, as discussed in the introduction. Indeed, based on previous water intrusion studies on the hydrophobic zeolite silicalite-1, aqueous PLs based on this material, such as that recently reported,^[22] should also exhibit high compressibility, albeit at higher pressures than those described here. Compared to ZIF-8E-based PLs with equivalent weight-content, the degree of compression should be lower, however, due to the lower gravimetric pore volume of silicalite-1 ($0.2 \text{ cm}^3 \text{ g}^{-1}$ vs $0.57 \text{ cm}^3 \text{ g}^{-1}$ for ZIF-8).^[37] We further anticipate that related strategies can generate compressible liquids based on Type-I and Type-II porous liquids, either based on cavity collapse or forced cavity occupation, and further studies of physical aspects such as shock absorption and acoustic properties will be of interest.

Supporting Information

Supporting Information is available from the Wiley Online Library or from the author.

Conflict of Interest

The authors declare no conflict of interest.

Data Availability Statement

The data that support the findings of this study are available from the corresponding author upon reasonable request.

Keywords

compressible liquids, hydrophobicity, neutron scattering, porous liquids, ZIF

Received: July 4, 2023
Revised: August 12, 2023
Published online: September 20, 2023

- [1] M. Crocker, *Handbook of Acoustics*, (Ed: J. Malcolm), John Wiley & Sons, New York **1998**.
- [2] S. Ridah, *J. Appl. Phys.* **1988**, *64*, 152.
- [3] G. S. Kell, *J. Chem. Eng. Data* **1970**, *15*, 119.
- [4] N. O'Reilly, N. Giri, S. L. James, *Chemistry* **2007**, *13*, 3020.
- [5] D. Wang, Y. Xin, D. Yao, X. Li, H. Ning, H. Zhang, Y. Wang, X. Ju, Z. He, Z. Yang, W. Fan, P. Li, Y. Zheng, *Adv. Funct. Mater.* **2022**, *32*, 2104162.
- [6] P. G. Yot, L. Vanduyfhuys, E. Alvarez, J. Rodriguez, J.-P. Itié, P. Fabry, N. Guillou, T. Devic, I. Beurroies, P. L. Llewellyn, V. V. Speybroeck, C. Serre, G. Maurin, *Chem. Sci.* **2015**, *7*, 446.
- [7] G. Ortiz, H. Nouali, C. Marichal, G. Chaplais, J. Patarin, *Phys. Chem. Chem. Phys.* **2013**, *15*, 4888.
- [8] Y. Sun, S. M. J. Rogge, A. Lamaire, S. Vandenbrande, J. Wieme, C. R. Siviour, V. Van Speybroeck, J.-C. Tan, *Nat. Mater.* **2021**, *20*, 1015.
- [9] Y. Sun, Y. Li, J.-C. Tan, *Phys. Chem. Chem. Phys.* **2018**, *20*, 10108.
- [10] Y. Sun, Y. Li, J.-C. Tan, *ACS Appl. Mater. Interfaces* **2018**, *10*, 41831.
- [11] M. Tortora, P. Zajdel, A. R. Lowe, M. Chorążewski, J. B. Leão, G. V. Jensen, M. Bleuél, A. Giacomello, C. M. Casciola, S. Meloni, Y. Grosu, *Nano Lett.* **2021**, *21*, 2848.
- [12] Y. Grosu, V. Eroshenko, J. M. Nedelec, J. P. E. Grolier, *Phys. Chem. Chem. Phys.* **2015**, *17*, 1572.
- [13] Y. A. Grosu, G. Renaudin, V. Eroshenko, J.-M. Nedelec, J.-P. E. Grolier, *Nanoscale* **2015**, *7*, 8803.
- [14] Y. Grosu, S. Gomes, G. Renaudin, J.-P. E. Grolier, V. Eroshenko, J.-M. Nedelec, *RSC Adv.* **2015**, *5*, 89498.
- [15] V. Eroshenko, R.-C. Regis, M. Souldard, J. Patarin, *J. Am. Chem. Soc.* **2001**, *123*, 8129.
- [16] I. Khay, G. Chaplais, H. Nouali, C. Marichal, J. Patarin, *RSC Adv.* **2015**, *5*, 31514.
- [17] I. Khay, G. Chaplais, H. Nouali, G. Ortiz, C. Marichal, J. Patarin, *Dalton Trans.* **2016**, *45*, 4392.
- [18] M. Michelin-Jamois, C. Picard, G. Vigier, E. Charlaix, *Phys. Rev. Lett.* **2015**, *115*, 036101.
- [19] J. C. Tan, T. D. Bennett, A. K. Cheetham, *Proc. Natl. Acad. Sci. USA* **2010**, *107*, 9938.
- [20] J.-P. Zhang, A.-X. Zhu, R.-B. Lin, X.-L. Qi, X.-M. Chen, *Adv. Mater.* **2011**, *23*, 1268.
- [21] E. E. Sann, Y. Pan, Z. Gao, S. Zhan, F. Xia, *Sep. Purif. Technol.* **2018**, *206*, 186.
- [22] D. P. Erdosy, M. B. Wenny, J. Cho, C. DelRe, M. V. Walter, F. Jiménez-Ángeles, B. Qiao, R. Sanchez, Y. Peng, B. D. Polizzotti, M. O. de la Cruz, J. A. Mason, *Nature* **2022**, *608*, 712.
- [23] A. Pichon, A. Lazuen-Garay, S. L. James, *CrystEngComm* **2006**, *8*, 211.
- [24] D. Crawford, J. Casaban, R. Haydon, N. Giri, T. McNally, S. L. James, *Chem. Sci.* **2015**, *6*, 1645.
- [25] Y. Zhang, *Mechanochemical Synthesis of Metal-Organic Frameworks, Ph.D thesis*, Queen's University Belfast, Belfast, UK **2017**.
- [26] Zinc carbonate basic, <https://www.americanelements.com/zinc-carbonate-basic-5263-02-5> (accessed: July 2023).
- [27] X. Ma, W. Yuan, S. E. J. Bell, S. L. James, *Chem. Commun.* **2014**, *50*, 1585.
- [28] G. Ortiz, H. Nouali, C. Marichal, G. Chaplais, J. Patarin, *J. Phys. Chem. C* **2014**, *118*, 7321.

- [29] S. A. Moggach, T. D. Bennett, A. K. Cheetham, *Angew. Chem., Int. Ed.* **2009**, *48*, 7087.
- [30] B. Lefevre, A. Saugey, J. L. Barrat, L. Bocquet, E. Charlaix, P. F. Gobin, G. Vigier, *J. Chem. Phys.* **2004**, *120*, 4927.
- [31] R. Boada, S. Diaz-Moreno, S. E. Norman, D. T. Bowron, *Mol. Phys.* **2019**, *117*, 3456.
- [32] J. G. Vitillo, L. Gagliardi, *Chem. Mater.* **2021**, *33*, 4465.
- [33] T. Youngs, *Mol. Phys.* **2019**, *117*, 3464.
- [34] C. L. Hobday, C. H. Woodall, M. J. Lennox, M. Frost, K. Kamenev, T. Düren, C. A. Morrison, S. A. Moggach, *Nat. Commun.* **2018**, *9*, 1429.
- [35] M.-C. Bellissent-Funel, L. Bosio, *J. Chem. Phys.* **1995**, *102*, 3727.
- [36] B. D. Egleston, A. Mroz, K. E. Jelfs, R. L. Greenaway, *Chem. Sci.* **2022**, *13*, 5042.
- [37] E. M. Flanigen, J. M. Bennett, R. W. Grose, J. P. Cohen, R. L. Patton, R. M. Kirchner, J. V. Smith, *Nature* **1978**, *271*, 512.